On-Chip Tunable Second-Order Differential-Equation Solver Based on a Silicon Photonic Mode-Split Microresonator

Jiayang Wu, Boyu Liu, Jizong Peng, Junming Mao, Xinhong Jiang, Ciyuan Qiu, Christine Tremblay, *Member, IEEE, Member, OSA*, and Yikai Su, *Senior Member, IEEE, Member, OSA*

***Abstract*—We propose and experimentally demonstrate an on-chip all-optical differential-equation solver capable of solving second-order ordinary differential equations (ODEs) characterizing continuous-time linear time-invariant systems. The photonic device is implemented by a self-coupled microresonator on a silicon-on-insulator platform with mutual coupling between the cavity modes. Owing to the mutual mode coupling within the same resonant cavity, the resonance wavelengths induced by different cavity modes are self-aligned, thus avoiding precise wavelength alignment and unequal thermal wavelength drifts as in the case of cascaded resonators. By changing the mutual mode coupling strength, the proposed device can be used to solve second-order ODEs with tunable coefficients. System demonstration using the fabricated device is carried out for 10-Gb/s optical Gaussian and super-Gaussian input pulses. The experimental results are in good agreement with theoretical predictions of the solutions, which verify the feasibility of the fabricated device as a tunable second-order photonic ODE solver.**

***Index Terms*—Differential-equation solver, mode splitting, resonators, silicon photonics.**

I. Introduction

DIFFERENTIAL equations, as the language expressing the laws of nature, model a large variety of fundamental phenomena and find applications in almost any discipline of science and engineering [1]. Constant-coefficient linear ordinary differential equations (ODEs) are basic differential equations used to describe continuous-time linear time-invariant (LTI) systems, which are classical models in the theory of signals and systems [2]. Solving ODEs is widely required in real-time information processing, classic mechanics, control theory, chemical kinetics, weather forecasting, and so forth [3]–[6]. Performing ODE solving in optical domain could overcome the bandwidth bottleneck in electronic processing and provide processing speed orders of magnitude higher than the electronic counterparts [7], [8], thus holding great promise for high-speed computing and information processing.

Various schemes have been proposed to realize all-optical ODE solvers based on semiconductor optical amplifiers [9], [10], fiber gratings [11], [12], and silicon photonic integrated circuits (PICs) [13]–[17]. Amongst them, the ODE solvers based on silicon PICs are very attractive since they could offer competitive advantages of micro-scale footprint, low power consumption, capability of large-scale integration, and compatibility with well-developed silicon fabrication technologies. In previous reports, first-order ODE solvers implemented by on-chip silicon micro-ring resonators (MRRs) were demonstrated [16], [17]. On the other hand, high-order ODE solvers performing more powerful computing and processing functionalities are also of great significance in characterization of more complicated high-order systems. Second-order silicon photonic ODE solvers were studied in [15], [17]. These ODE solvers were implemented by multiple cascaded resonators, which impose stringent requirements on the alignment of resonance wavelengths from separate resonators [18]. It is also quite challenging to maintain the desired spectra in consideration of unequal wavelength drifts induced by nonlinear thermo-optic effect [19], [20]. Moreover, the demonstrations of the ODE solvers in [15], [17] were performed with fixed values of constant coefficients, while tunability is desired in practical applications.

Mode-splitting occurs when two or more mutually coupled modes co-exist in one resonant cavity [21]. It is a common phenomenon in resonators, which can lead to various meaningful transmission spectra including electromagnetically-induced-transmission -like transmission [22], electromagnetically-induced-absorption -like transmission [23], and Fano transmission [24]. In our previous work, mode splitting in coupled cavity systems was theoretically analyzed in spectral domain [25] and experimentally demonstrated based on sidewall-roughness-induced reflection in a MRR [21], [26]. In this paper, for the first time to the best of our knowledge, mode splitting within a single resonant cavity is characterized in the time domain and exploited for ODE solving. A self-coupled micro-resonator with tunable mutual mode coupling is proposed and demonstrated as a tunable ODE solver for continuous-time LTI systems. Benefitting from the self-aligned resonances in this mode-split resonator, precise alignment of resonance wavelengths is not necessary and unequal thermal wavelength drifts can also be avoided. Different

Manuscript received February 16, 2015; revised May 28, 2015; accepted June 5, 2015. Date of publication June 11, 2015; date of current version August 3, 2015. This work was supported in part by the National Natural Science Foundation of China under Grant 61125504/61235007, and the 863 High-Tech Program under Grant 2015AA015503/2015AA017001.

J. Wu, B. Liu, J. Peng, J. Mao, X. Jiang, C. Qiu, and Y. Su are with the State Key Laboratory of Advanced Optical Communication Systems and Networks, Department of Electronic Engineering, Shanghai Jiao Tong University, Shanghai 200240, China (e-mail: jiayangwu@sjtu.edu.cn; charlesliu@sjtu.edu.cn; pengjizong@sjtu.edu.cn; jeremymao@sjtu.edu.cn; jiangxinhong@sjtu.edu.cn; qiuciyuan@sjtu.edu.cn; yikaisu@sjtu.edu.cn).

C. Tremblay is with the Laboratoire de technologies de réseaux, École de technologie supérieure, Montreal, QC H3C 1K3, Canada (e-mail: christine.tremblay@etsmtl.ca).

Color versions of one or more of the figures in this paper are available online at http://ieeexplore.ieee.org.

Digital Object Identifier 10.1109/JLT.2015.2442911

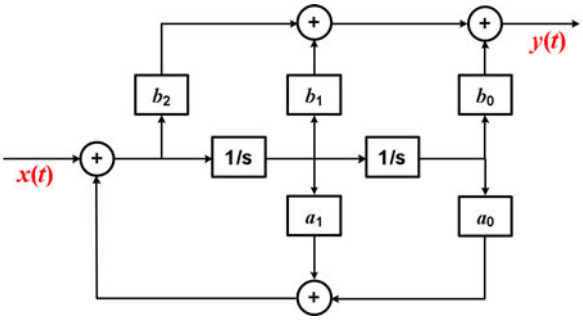

Fig. 1. (Color online) Block diagram of the LTI system corresponding to Eq. (2). 1/*s* denotes the system function of an integrator in the Laplace transform.

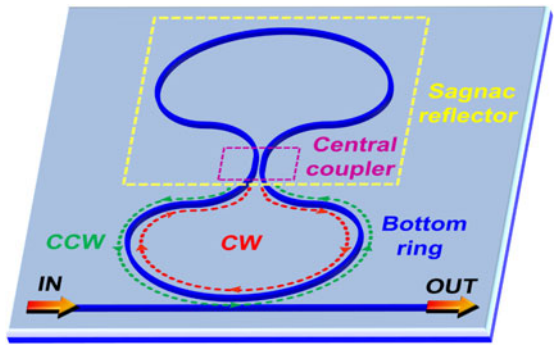

Fig. 2. (Color online) Schematic configuration of the proposed self-coupled resonator with mutual mode coupling between the clockwise (CW) and counter-clockwise (CCW) modes in the bottom ring induced by the upper Sagnac reflector.

from the mode splitting caused by sidewall roughness, the mutual mode coupling in the proposed device can be dynamically changed by a thermally-tuned central interferometric coupler, whereby tunable constant coefficients of the ODE are achieved. The proposed device is fabricated, and system demonstration of solving ODE is performed using 10-Gb/s optical Gaussian and super-Gaussian input pulses. The experimental results validate the effectiveness of the proposed device as an on-chip tunable second-order ODE solver.

II. Device Configuration and Operation Principle

From the classical theory of signals and systems, all continuous-time LTI systems can be characterized by a linear constant-coefficient ODE normalized as [2]:

$$\frac{d^n y(t)}{dt^n} + a_{n-1}\frac{d^{n-1}y(t)}{dt^{n-1}} + \ldots + a_1\frac{dy(t)}{dt} + a_0 y(t) = b_m\frac{d^m x(t)}{dt^m} + b_{m-1}\frac{d^{m-1}x(t)}{dt^{m-1}} + \ldots + b_1\frac{dx(t)}{dt} + b_0 x(t), \tag{1}$$

where $x(t)$ is the system input signal, and $y(t)$ is the solution of the ODE as the system output signal. a_i $(i = 0, 1, \ldots, n-1)$ and b_k $(k = 0, 1, 2, \ldots, m)$ are constant coefficients. In Eq. (1), $m \le n$ and $a_i \ge 0$ $(i = 0, 1, \ldots, n-1)$ should be satisfied due to the stability and the causality of practical systems. In terms of second-order condition, Eq. (1) can be written as:

$$\frac{d^2 y(t)}{dt^2} + a_1\frac{dy(t)}{dt} + a_0 y(t) = b_2\frac{d^2 x(t)}{dt^2} + b_1\frac{dx(t)}{dt} + b_0 x(t), \tag{2}$$

Compared to the second-order ODE in [14], there are additional derivative terms of the input signal in Eq. (2), thus allowing more general and versatile characterization of LTI systems. The block diagram of the LTI system corresponding to Eq. (2) is shown in Fig. 1, which consists of a certain number of adders, integrators/differentiators, and scalar multipliers [2].

Fig. 2 illustrates the schematic configuration of the proposed self-coupled resonator with mutual mode coupling, which consists of a self-coupled resonant loop and a bus waveguide. The bus waveguide is side-coupled to the resonant loop and serves as system input and output channels. The upper part of the resonant loop together with the central coupler can be regarded as a Sagnac reflector [27], which excites back-reflection of the input light and induce mutual coupling between the clockwise (CW) and counter-clockwise (CCW) modes in the bottom ring. Using the coupled mode theory [21], [28], we obtain the spectral transfer function around any given resonance of the proposed self-coupled resonator as follows:

$$T(\omega) = \frac{[j(\omega-\omega_0)]^2 + b_1 j(\omega-\omega_0) + b_0}{[j(\omega-\omega_0)]^2 + a_1 j(\omega-\omega_0) + a_0}. \tag{3}$$

In Eq. (3), $j = \sqrt{-1}$, ω is the angular frequency variable, and $\omega_0 = 2\pi c/\lambda_0$ is the resonance angular frequency, with c and λ_0 denoting the light speed in vacuum and the resonance wavelength. a_0, a_1, b_0, and b_1 are constant coefficients which can be given by:

$$\begin{cases} a_1 = \omega_0(1/Q_i + 1/Q_e), \\ a_0 = \omega_0^2\left[(1/Q_i + 1/Q_e)^2 + 1/Q_u^2\right]/4, \\ b_1 = \omega_0/Q_i, \\ b_0 = \omega_0^2\left[1/Q_i^2 - 1/Q_e^{22} + 1/Q_u^2\right]/4, \end{cases} \tag{4}$$

where Q_i, Q_e, and Q_u denote the quality factors related to internal cavity loss, external coupling between the self-coupled resonant loop and the bus waveguide, and mutual coupling between the CW and CCW modes, respectively. For $Q_u \to \infty$, $T(\omega)$ in Eq. (3) reduces to the transfer function of a single MRR [17]. Here a critical mutual coupling quality factor Q_{uc} satisfying $1/Q_{uc}^2 = |1/Q_e^2 - 1/Q_i^2|$ is defined. In the case of $Q_i > Q_e$, i.e., $1/Q_{uc}^2 = 1/Q_e^2 - 1/Q_i^2$, $T(\omega_0)$ in Eq. (3) equals to 0 when $Q_u = Q_{uc}$. The normalized transmission spectra and phase responses for various Q_u in this case are shown in Fig. 3(a) and (b), respectively. For $Q_u > Q_{uc}$, the transmission spectra and phase responses are close to those of single MRRs in the over-coupling regime [29], and the discrepancies increase with the decreasing of Q_u. Resonance splitting occurs when $Q_u < Q_{uc}$. Decreased Q_u leads to increased mode splitting degree, i.e., the spectral range between the split resonances. Under the condition of $Q_i < Q_e$, i.e., $1/Q_{uc}^2 = 1/Q_i^2 - 1/Q_e^2$, $T(\omega_0)$ in Eq. (3) increases with the decreasing of Q_u and changes away from 0. The transmission spectra and phase responses in Fig. 3(c) and (d) under such condition are close to those of

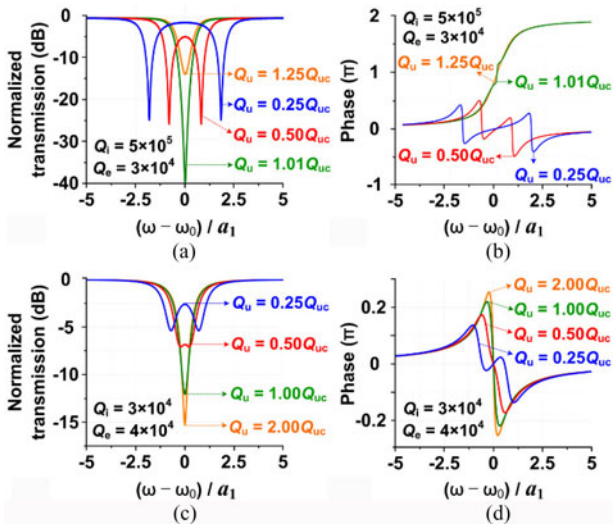

Fig. 3. (Color online) (a) Normalized transmission spectra and (b) phase responses of the proposed mode-split resonator for various Q_u when $Q_i = 5 \times 10^5$ and $Q_e = 3 \times 10^4$. (c) Normalized transmission spectra and (d) phase responses for various Q_u when $Q_i = 3 \times 10^4$ and $Q_e = 4 \times 10^4$.

single MRRs in the under-coupling regime [29], with increased discrepancies for decreased Q_u. Resonance splitting also takes place when $Q_u < Q_{uc}$ and enhanced with the decreasing of Q_u. It should be noted that the mode splitting in [21] is caused by the fabrication-induced sidewall roughness, and hence it is difficult to control the mode splitting degree. Whereas for the proposed self-coupled resonator, varied Q_u can be obtained by changing the reflectivity of the Sagnac loop, i.e., the coupling strength of the central coupler, thus leading to tunable mode splitting degree with variable filtering shape. Increased coupling strength of the central coupler means decreased Q_u, thus resulting in enhanced resonance splitting with increased spectral range between the split notches.

For an input optical signal $X(t) = x\,(t)\,e^{j\omega_0 t}$ with a complex envelope of $x(t)$ at the carrier angular frequency of ω_0, the system output signal $Y(t) = y\,(t)\,e^{j\omega_0 t}$ is related to the input signal in spectral domain by:

$$T(\omega) = \frac{Y_F(\omega)}{X_F(\omega)} = \frac{y_F(\omega-\omega_0)}{x_F(\omega-\omega_0)} = \frac{[j(\omega-\omega_0)]^2 + b_1 j(\omega-\omega_0) + b_0}{[j(\omega-\omega_0)]^2 + a_1 j(\omega-\omega_0) + a_0}, \quad (5)$$

where $y(t)$ is the complex envelope of the output optical signal. $X_F(\omega)$, $x_F(\omega)$, $Y_F(\omega)$, and $y_F(\omega)$ are the Fourier transforms of $X(t)$, $x(t)$, $Y(t)$, and $y(t)$, respectively. After inverse Fourier transformation [2] from Eq. (5), we obtain a temporal ODE which can be expressed as:

$$\frac{d^2y(t)}{dt^2}e^{j\omega_0 t} + a_1\frac{dy(t)}{dt}e^{j\omega_0 t} + a_0 y(t)e^{j\omega_0 t} = \frac{d^2x(t)}{dt^2}e^{j\omega_0 t} + b_1\frac{dx(t)}{dt}e^{j\omega_0 t} + b_0 x(t)e^{j\omega_0 t}, \quad (6)$$

After eliminating the common factor $e^{j\omega_0 t}$, Eq. (6) can be further simplified to:

$$\frac{d^2y(t)}{dt^2} + a_1\frac{dy(t)}{dt} + a_0 y(t) = \frac{d^2x(t)}{dt^2} + b_1\frac{dx(t)}{dt} + b_0 x(t). \quad (7)$$

Eq. (7) has a form similar to the general second-order ODE in Eq. (2), meaning that the mode-split resonator could be characterized by a second-order ODE in time domain and employed as a second-order ODE solver. The constant coefficient of $d^2x(t)/dt^2$ determining the amplitude of the output signal is normalized to 1 with respect to passive filters. Given that there are other amplifications or attenuations in practical processing, the difference in amplitude can be further compensated. The differential item dt corresponds to the round-trip transit time in the resonant cavity, which is typically in unit of picosecond for silicon micro-resonator. The constant coefficients a_0, a_1, b_0, and b_1 determined by Q_i, Q_e, and Q_u compensate the magnitude of $1/dt$ and $1/dt^2$, therefore the proposed ODE solver is capable of processing high-speed optical signals. Once the second-order ODE to be solved is known, i.e., the values of a_1, a_0, b_1, b_0 are given, one can obtain the values of Q_i, Q_e, and Q_u according to Eq. (4), and then design the device similar to that in [17], [25]. Tunable constant coefficients of the ODE in Eq. (7) can be achieved by changing Q_i, Q_e, or Q_u. The calculated coefficients a_1, b_1, a_0, and b_0 of the ODE in Eq. (7) for various Q_i and Q_e are depicted in Fig. 4(a), (b), (c), and (d), respectively. ω_0 is assumed to be $\sim 1.2161 \times 10^{15}$, which corresponds to the wavelength of $\lambda_0 = 1550$ nm. a_1 and b_1 are in unit of s^{-1}, while a_0 and b_0 are in unit of s^{-2}.The tuning of Q_e and effective Q_i can be achieved using the same method as that was demonstrated in our previous work [17]. In this paper, we mainly focus on the tuning of Q_u. The variation of Q_u would lead to the changes of the coefficients a_0 and b_0. Fig. 4(e) and (f) illustrate the calculated coefficients a_0 and b_0 of the ODE in Eq. (7) for various Q_u/Q_{uc} under different conditions of Q_i and Q_e. It can be seen that a larger difference between Q_i and Q_e results in a broader tunable range of the two coefficients.

As for the second-order ODE solver implemented by two cascaded MRRs in [17], precise alignment of the resonance wavelengths from separate MRRs is required. Moreover, all the constant coefficients a_0, a_1, b_0, and b_1 are the functions of four variables determined by the two MRRs. As a result, changing of any variable would lead to variations of all the four coefficients. If one wants to change one of these coefficients, it is required to adjust all the four quality factors simultaneously and keep accurate matching of their variations. Whereas for a second-order ODE solver based on the proposed mode-split resonator, precise alignment of the resonance wavelength is not necessary since the resonator itself can co-excite two degenerate modes in one cavity with the same resonance wavelengths. Besides, the number of variables that determine the constant coefficients a_0, a_1, b_0, and b_1 are 3, 2, 3, and 1, respectively. The proposed scheme for ODE solving could be extended to solve higher order ODEs by cascading multiple devices [15] or by employing higher-order resonant filters with interactions between multiple cavity modes [30], [31].

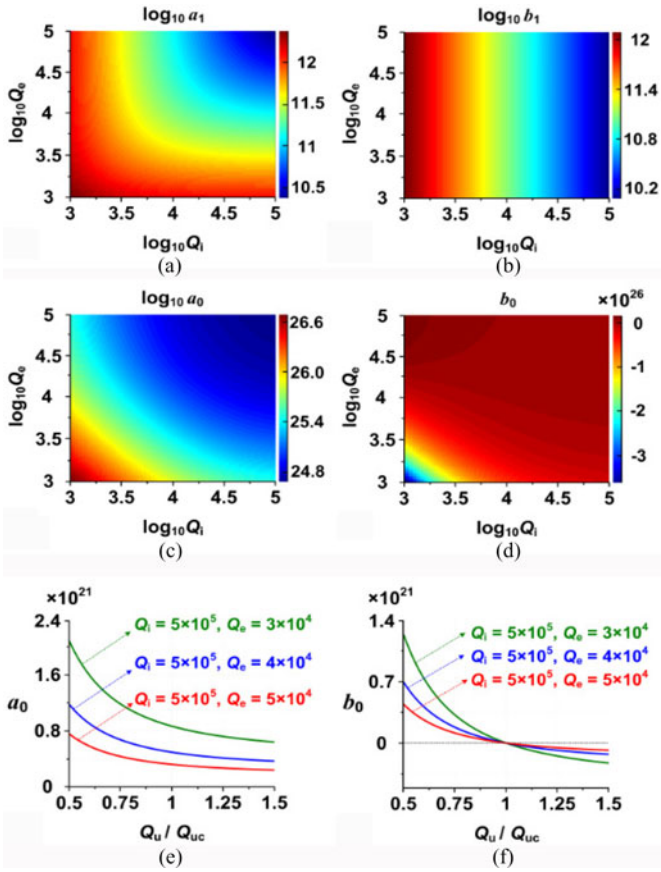

Fig. 4. (Color online) Calculated coefficients (a) a_1, (b) b_1, (c) a_0, and (d) b_0 of the ODE in Eq. (7) for various Q_i and Q_e when $Q_u = 1 \times 10^4$. (e) Calculated coefficients a_0 and (f) b_0 of the ODE in Eq. (7) for various Q_u / Q_{uc} under various conditions of Q_i and Q_e.

III. Device Fabrication and Measured Spectra

The designed ODE solver based on the above principle was fabricated on a commercial SOI wafer with 220-nm-thick top silicon layer. The entire fabrication process was CMOS compatible. A micrograph of the fabricated device is shown in Fig. 5(a). The device pattern was defined by 248-nm deep-ultraviolet (DUV) photolithography, and the top silicon layer was etched by an inductively coupled plasma etching process. The central directional coupler in Fig. 2 is replaced by an interferometric coupler, thus the effective coupling strength can be changed by thermally tuning the phase shift along one arm using a micro-heater [17]. The fabrication of the thermo-optic micro-heater was in a process similar to that in [17]. The gap size in the straight coupling regions is ~180 nm due to the resolution of 248-nm DUV photolithography. The cross sections of the single-mode silicon waveguides are 500×220 nm^2, and the straight coupling length between the resonant loop and the bus waveguide is ~3 μm. This is aimed to increase the difference between Q_i and Q_e, thus leading to increased tuning range of the constant coefficients. TE-polarized grating couplers were fabricated at the ends of the input and output channels to couple light into and out of the chip with single mode fibers.

The measured transmission spectrum of the fabricated device is shown in Fig. 5(b) by the solid curve. The on-chip insertion loss is measured to be ~13 dB. The theoretically fitted spectrum obtained from Eq. (3) is shown by the dashed curve. Similar to that in our previous reports [25], [26], we firstly calculated $\omega_0 = 2\pi c/\lambda_0$, and then fitted the spectrum with proper values of Q_i, Q_e, and Q_u to minimize the difference between the theoretical and measured curves. The fitting parameters are $Q_i = \sim 7.93 \times 10^4$, $Q_e = \sim 1.27 \times 10^4$, and $Q_u = \sim 9.68 \times 10^3$. The average deviation defined as the mean absolute deviation of the measured spectrum from the fitted one in Fig. 5(b) is ~2.3%. The calculated a_0, a_1, b_0, and b_1 using these fitting parameters are also presented in Fig. 5(b). By applying a direct-current (DC) voltage to the micro-heater along one arm of the interferometric coupler, tunable mode splitting can be obtained. When the DC voltages applied to the micro-heater are 1.2, 2.0, 2.5, and 3.5 V, i.e., the heating powers are 3.2, 8.9, 13.9, and 27.2 mW, the measured transmission spectra are shown in Fig. 5(c), (d), (e) and (f), respectively. The fitted spectra with the same Q_i and Q_e but different Q_u are also provided. Since the interferometric coupler is part of the resonant loop, the applied DC voltages also cause a slight red shifting of the spectra shown in Fig. 5(b)–(f). By employing push-pull phase shifters along both arms of the central interferometric coupler [32], such shifting can be reduced. The slight red shifting of the resonance wavelength induced by thermo-optic tuning was neglected in the calculations of the four coefficients since it caused negligible differences. The average deviations in Fig. 5(c)~(f) are ~2.5%, ~2.6%, ~2.9%, and ~2.8%, respectively. One can see that Q_u increases with raised voltage, resulting in the changing of a_0 and b_0. As the applied voltage increases, the spectral range between the split notches decreases until the split notches finally merge to a single one with increased depth. By further increasing the applied voltage, the depth of the combined single notch decreases.

IV. System Demonstration of Solving ODE With Tunable Coefficients

Fig. 6 illustrates the schematic diagram of the experimental setup used for system demonstration of a tunable ODE solver. A continuous-wave (CW) light from a tunable laser with a tuning resolution of 0.01 nm is used as an optical carrier. Optical Gaussian and super-Gaussian pulses are employed as typical input pulse waveforms in our experiment. The optical super-Gaussian pulses are generated by driving a Mach-Zehnder modulator (MZM) biased at the quadrature point of the transmission curve using a 10-Gb/s electrical non-return-to-zero (NRZ) signal. The NRZ signal with a pattern of "10000000" is generated by a pulse pattern generator (PPG) and then amplified by an electrical amplifier (EA). The optical Gaussian pulses are obtained by cascading one more MZM driven by a 10-GHz clock signal from the PPG to carve the generated super-Gaussian pulses [33]. A tunable electrical tunable phase shifter (EPS) is utilized to synchronize the super-Gaussian pulses and the clock signal, thus optimizing the carving effect. The generated input optical signal is boosted by an erbium-doped fiber amplifier (EDFA),

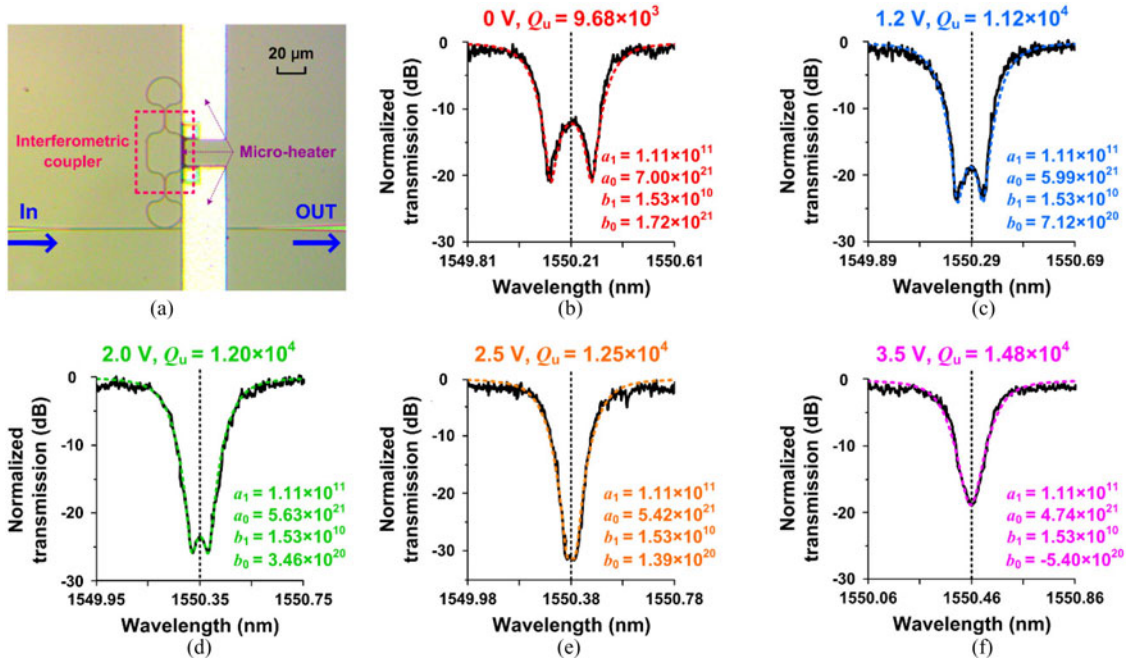

Fig. 5. (Color online) (a) Micrograph of the fabricated device. (b)–(f) Measured (solid curves) and fitted (dashed curves) transmission spectra of the device in (a) when the DC voltages applied to the micro-heater are 0, 1.2, 2.0, 2.5, and 3.5 V, respectively. The dashed vertical lines illustrate symmetry axes.

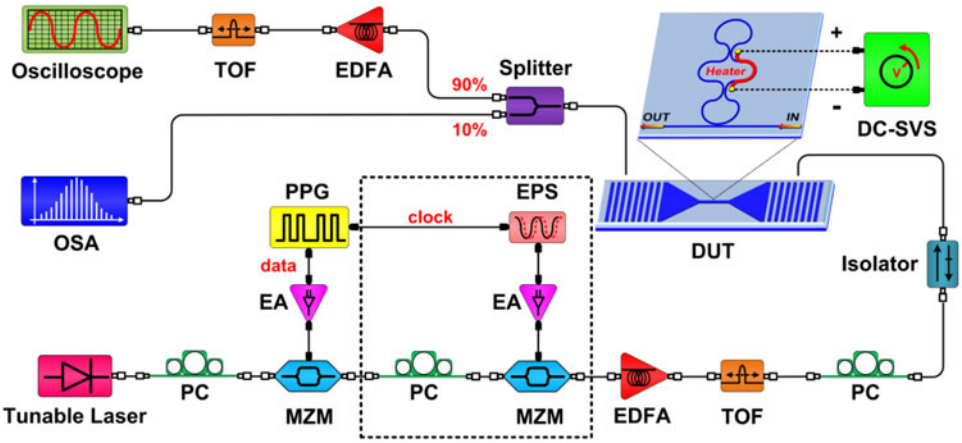

Fig. 6. (Color online) Experimental setup for system demonstration. PC: polarization controller. PPG: pulse pattern generator. EA: electrical amplifier. MZM: Mach-Zehnder modulator. EPS: electrical phase shifter. EDFA: erbium-doped fiber amplifier. TOF: tunable optical filter. DUT: device under test. DC-SVS: direct-current stabilized voltage source. OSA: optical spectrum analyzer. The dashed box shows additional facilities used to generate optical Gaussian pulses.

followed by a tunable band pass filter (BPF) to suppress the amplified spontaneous emission (ASE) noise. A polarization controller (PC) is inserted before the device under test (DUT) to minimize the coupling loss induced by the TE-polarized grating couplers. An optical isolator is employed to prevent the reflected light from damaging the laser source. The output signal from the DUT is split into two parts using a fiber optic power splitter. One part is fed into an optical spectrum analyzer (OSA), and the other part is sent to an oscilloscope after being amplified by another EDFA together with one more BPF to suppress the ASE noise.

We first demonstrate the effectiveness of solving second-order ODE. The temporal waveform of the generated 10-Gb/s optical Gaussian input pulse and the theoretically fitted trace are depicted in Fig. 7(a) by the solid and dashed curves, respectively. The observed temporal waveform of the output signal from the DUT is shown in Fig. 7(b). The wavelength of the CW light from the tunable laser is aligned to the symmetry axis in Fig. 5(b). The theoretically calculated waveform according to the solution of the ODE in Eq. (7) with constant coefficients a_0, a_1, b_0, and b_1 equaling to those in Fig. 5(b) is also shown in Fig. 7(b) for comparison. As the input optical signal in the experiment is hard to reproduce exactly in the simulations, we assume ideal Gaussian pulses as the input signals in the simulations. One can see that the observed output waveform in Fig. 7(b) matches closely with the calculated one, except for slight discrepancies

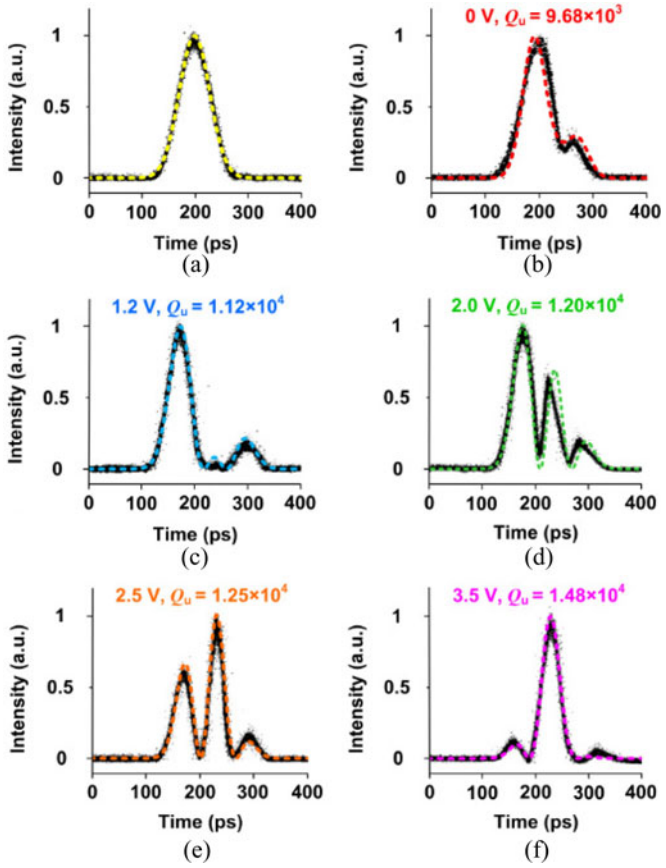

Fig. 7. (Color online) (a) Experimentally observed (solid curve) and theoretically fitted (dashed curve) 10-Gb/s optical Gaussian input pulse. (b)–(f) Experimentally observed output pulse waveforms (solid curves) and theoretically calculated pulse waveforms indicating the solutions of the ODE in Eq. (7) (dashed curves) when the DC voltages applied to the micro-heater are 0, 1.2, 2.0, 2.5, and 3.5 V, respectively.

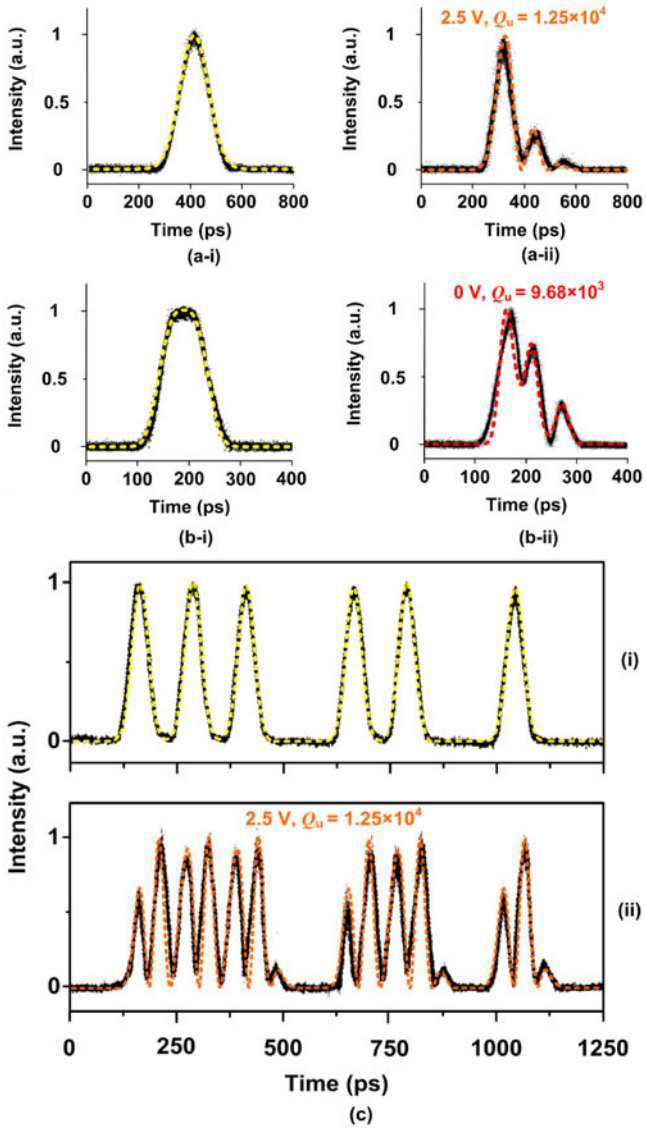

Fig. 8. (Color online) (a) Experimentally observed (i) 5-Gb/s optical Gaussian input pulse and (ii) output pulse waveform with 2.5 V DC voltage applied to the micro-heater. (b) Experimentally observed (i) 10-Gb/s optical super-Gaussian ($m = 3$) input pulse and (ii) output pulse waveform with zero voltage applied to the micro-heater. (c) Experimentally observed (i) 10-Gb/s optical Gaussian input pulse train and (ii) output pulse waveform with 2.5 V DC voltage applied to the micro-heater. The theoretical calculated pulse waveforms are illustrated by the dashed curves in (a)–(c) accordingly.

that can be attributed to the imperfect Gaussian input pulse in the experiment. The average deviation of the measured waveform from the numerical solution of the ODE is ∼3.8%. We then demonstrate the tunability of the fabricated ODE solver. When the voltages applied to the micro-heater are 1.2, 2.0, 2.5, and 3.5 V, corresponding to the measured spectra in Fig. 5(c), (d), (e), and (f), the experimentally observed temporal waveforms of the output signals are depicted in Figs. 7(c), (d), (e), and (f), respectively. The optical carrier wavelength is slightly tuned to align with the symmetry axes in Fig. 5(c)–(f). The dashed waveforms corresponding to the theoretical solutions of the ODE in Eq. (7) with a_0, a_1, b_0, and b_1 equaling to those in Fig. 5(c)–(f) are also shown. The observed output waveforms in Fig. 7(c)–(f) also show good agreement with theoretical solutions of the ODE in Eq. (7). The average deviations are ∼3.5%, ∼4.2%, ∼3.3%, and ∼3.6%, respectively. The agreement between the experimental results and the theoretical predictions of the solutions verifies the effectiveness of the proposed device as a tunable second-order photonic ODE solver.

When we further change the data rate of the optical Gaussian input pulse to 5 Gb/s, the experimentally observed and theoretically calculated output pulse waveforms are shown in Fig. 8(a-ii) by the solid and dashed curves, respectively. The calculated pulse waveform indicates the solution of the ODE in Eq. (7) with a_0, a_1, b_0, and b_1 equaling to those in Fig. 5(e). The DC voltage applied to the micro-heater is 2.5 V. Here we chose 2.5 V applied voltage the same as in the case of Fig. 5(e) to clearly show the difference between the pulse shapes of the 10 and 5-Gb/s output signals. The observed output pulse waveform in Fig. 8(a-ii) agrees well with the calculated one, and differs from that in Fig. 7(e). The average deviation is ∼3.4%. Such agreement proves that the fabricated ODE solver is capable of processing optical signals at different rates. We also use 10-Gb/s super-Gaussian (m = 3) pulse shown in Fig. 8(b-i) as

an input. The experimentally observed output pulse waveform with zero applied voltage is shown in Fig. 8(b-ii). The calculated one corresponding to the solution of the ODE in Eq. (7) with a_0, a_1, b_0, and b_1 equaling to those in Fig. 5(b) is illustrated by the dashed curve. It can be seen that the experimentally observed output pulse waveform in Fig. 8(b-ii) closely approximates the theoretical trace. The average deviation is $\sim$4.2%. By using an electrical pseudo random bit sequence (PRBS) NRZ signal generated by the PPG to drive the first MZM in Fig. 6, we obtain optical Gaussian PRBS input pulse train shown in Fig. 8(c-i). The pattern length of the PRBS signal is 2^{31}–1. The corresponding output pulse waveform is shown in Fig. 8(c-ii), which also fits well with the theoretically calculated waveform with an average deviation of $\sim$4.6%. The experimental results in Figs. 8(b) and (c) confirm that the fabricated ODE solver can process various input pulse waveforms.

V. Conclusion

In summary, we have proposed and experimentally demonstrated an on-chip tunable photonic differential-equation solver that can be used to solve second-order ODEs characterizing continuous-time LTI systems. The photonic device based on a mode-split micro-resonator is monolithically integrated on a SOI wafer with a compact footprint of $\sim 25 \times 90\ \mu\text{m}^2$. The resonance wavelengths induced by different cavity modes within a same resonant cavity are self-aligned, whereby precise alignment of resonance wavelengths and unequal thermal wavelength drifts as in the case of cascaded resonators can be avoided. By changing the mutual mode coupling strength through a thermally-tuned interferometric coupler, varied mode splitting degree and tunable constant coefficients of the ODEs can be achieved. The feasibility of the fabricated device as a tunable ODE solver has been verified by system demonstration using 10-Gb/s optical Gaussian and super-Gaussian input pulses. The proposed device provide a new way to solve high-order differential equations in optical domain with reduced tuning complexity and improved stability, which could be a functional component for high-speed computing and information processing.

References

[1] G. F. Simmons, *Differential Equations With Applications and Historical Notes*. New York, NY, USA: McGraw-Hill, 1991.

[2] A. V. Oppenheim, A. S. Willsky, and S. Hamid, *Signals and Systems*. Englewood Cliffs, NJ, USA: Prentice-Hall, 1996.

[3] V. Fock, "Eigentime in classical and quantum mechanics," *Izv. USSR Acad. Sci. (Phys.)*, vol. 12, pp. 404–425, Apr. 1937.

[4] R. DiPerna and P. Lions, "Ordinary differential equations, transport theory and Sobolev spaces," *Invent. Math.*, vol. 98, no. 3, pp. 511–547, Oct. 1989.

[5] D. Shieh, Y. Chang, and G. Carmichael, "The evaluation of numerical techniques for solution of stiff ordinary differential equations arising from chemical kinetic problems," *Environ. Softw.*, vol. 3, no. 1, pp. 28–38, Mar. 1988.

[6] K. Ericksson, D. Estep, P. Hansbo, and C. Johnson, "Introduction to adaptive methods for differential equations," *Acta Numerica*, vol. 4, pp. 105–158, Jan. 1995.

[7] T. Elali, A. Sopeju, A. Fapohunda, and O. Olorode, "An analog computer to solve any first order linear differential equation with arbitrary coefficients," in *Proc. Ind. Electron., Technol. Autom.*, 2005, pp. 43–46.

[8] K. Y. Yun, P. A. Beerel, V. Vakilotojar, A. E. Dooply, and J. Arceo, "The design and verification of a high-performance low-control-overhead asynchronous differential equation solver," *IEEE Trans. Very Large Scale Integr. Syst.*, vol. 6, no. 4, pp. 643–655, Dec.1998.

[9] S. Tan, Z. Wu, L. Lei, S. Hu, J. Dong, and X. Zhang, "All-optical computing system for solving differential equations based on optical intensity differentiator," *Opt. Exp.*, vol. 21, no. 6, pp. 7008–7013, Mar. 2013.

[10] K. Chen, J. Hou, Z. Huang, T. Cao, J. Zhang, Y. Yu, and X. Zhang, "All-optical 1st- and 2nd-order differential equation solvers with large tuning ranges using Fabry-Pérot semiconductor optical amplifiers," *Opt. Exp.*, vol. 23, no. 3, pp. 3784–3794, Feb. 2015.

[11] J. Azaña, "Ultrafast analog all-optical signal processors based on fiber grating devices," *IEEE Photon. J.*, vol. 2, no. 3, pp. 359–386, Apr. 2010.

[12] R. Slavík, Y. Park, N. Ayotte, S. Doucet, T. Ahn, S. LaRochelle, and J. Azaña, "Photonic temporal integrator for all-optical computing," *Opt. Exp.*, vol. 16, no. 22, pp. 18202–18214, Apr. 2008.

[13] M. Ferrera, Y. Park, L. Razzari, B. E. Little, S. T. Chu, R. Morandotti, D. J. Moss, and J. Azaña, "On-chip CMOS-compatible all-optical integrator," *Nat. Commun.*, vol. 1, no. 29, pp. 1–5, Jun. 2010.

[14] L. Lu, J. Wu, T. Wang, and Y. Su, "Compact all-optical differential-equation solver based on silicon microring resonator," *Frontiers Optoelectron.*, vol. 5, no. 1, pp. 99–106, Mar. 2012.

[15] S. Tan, L. Xiang, J. Zou, Q. Zhang, Z. Wu, Y. Yu, J. Dong, and X. Zhang, "High-order all-optical differential equation solver based on microring resonators," *Opt. Lett.*, vol. 38, no. 19, pp. 3735–3738, Sep. 2013.

[16] T. Yang, J. Dong, L. Lu, L. Zhou, A. Zheng, X. Zhang, and J. Chen, "All-optical differential equation solver with constant-coefficient tunable based on a single microring resonator," *Sci. Rep.*, vol. 4, no. 5581, pp. 1–5, Jul. 2014.

[17] J. Wu, P. Cao, X. Hu, X. Jiang, T. Pan, Y. Yang, C. Qiu, C. Tremblay, and Y. Su, "Compact tunable silicon photonic differential-equation solver for general linear time-invariant systems," *Opt. Exp.*, vol. 22, no. 21, pp. 26254–26264, Oct. 2014.

[18] L. Zhou, T. Ye, and J. Chen, "Coherent interference induced transparency in self-coupled optical waveguide-based resonators," *Opt. Lett.*, vol. 36, no. 1, pp. 13–15, Jan. 2011.

[19] L. Fan, J. Wang, L. Varghese, H. Shen, B. Niu, Y. Xuan, A. Weiner, and M. Qi, "An all-silicon passive optical diode," *Science*, vol. 335, no. 6067, pp. 447–450, Jan. 2012.

[20] M. Xu, J. Wu, T. Wang, X. Hu, X. Jiang, and Y. Su, "Push–pull optical nonreciprocal transmission in cascaded silicon microring resonators," *IEEE Photon. J.*, vol. 5, no. 1, Feb. 2013.

[21] Z. Zhang, M. Dainese, L. Wosinski, and M. Qiu, "Resonance-splitting and enhanced notch depth in SOI ring resonators with mutual mode coupling," *Opt. Exp.*, vol. 16, no. 7, pp. 4621–4630, Mar. 2008.

[22] K. Totsuka, N. Kobayashi, and M. Tomita, "Slow light in coupled-resonator-induced transparency," *Phys. Rev. Lett.*, vol. 98, May 2007.

[23] K. Qu and G. Agarwal, "Phonon-mediated electromagnetically induced absorption in hybrid opto-electromechanical systems," *Phys. Rev. A*, vol. 87, Mar. 2013.

[24] Q. Zhang, X. Wen, G. Li, Q. Ruan, J. Wang, and Q. Xiong, "Multiple magnetic mode-based fano resonance in split-ring resonator/disk nanocavities," *ACS Nano*, vol. 7, no. 12, pp. 11071–11078, Nov. 2013.

[25] Q. Li, T. Wang, Y. Su, M. Yan, and M. Qiu, "Coupled mode theory analysis of mode-splitting in coupled cavity system," *Opt. Exp.*, vol. 18, no. 8, pp. 8367–8382, Apr. 2010.

[26] T. Wang, F. Liu, J. Wang, Z. Zhang, T. Ye, Y. Tian, M. Qiu, and Y. Su, "Pulse delay and advancement in SOI microring resonators with mutual mode coupling," *J. Lightw. Technol.*, vol. 27, no. 21, pp. 4734–4743, Nov. 2009.

[27] X. Sun, L. Zhou, J. Xie, Z. Zou, L. Lu, H. Zhu, X. Li, and J. Chen, "Tunable silicon Fabry–Perot comb filters formed by sagnac loop mirrors," *Opt. Lett.*, vol. 38, no. 4, pp. 567–569, Feb. 2013.

[28] C. Manolatou, M. Khan, S. Fan, P. Villeneuve, H. Haus, and J. Joannopoulos, "Coupling of modes analysis of resonant channel add-drop filters," *IEEE J. Quantum Electron.*, vol. 35, no. 9, pp. 1322–1331, Sep. 1999.

[29] J. Wu, P. Cao, X. Hu, T. Wang, M. Xu, X. Jiang, F. Li, L. Zhou, and Y. Su, "Nested configuration of silicon microring resonator with multiple coupling regimes," *IEEE Photon. Technol. Lett.*, vol. 25, no. 6, pp. 580–583, Mar. 2013.

[30] Z. Liu and R. Magnusson, "Concept of multiorder multimode resonant optical filters," *IEEE Photon. Technol. Lett.*, vol. 14, no. 8, pp. 1091–1093, Aug. 2002.

[31] A. Poon, F. Courvoisier, and R. Chang, "Multimode resonances in square-shaped optical microcavities," *Opt. Lett.*, vol. 26, no. 9, pp. 632–634, May 2001.

[32] P. Dong, L. Chen, and Y. Chen, "High-speed low-voltage single-drive push-pull silicon Mach-Zehnder modulators," *Opt. Exp.*, vol. 20, no. 6, pp. 6163–6169, Mar. 2012.
[33] P. J. Winzer and R. J. Essiambre, "Advanced optical modulation formats," *Proc. IEEE*, vol. 94, no. 5, pp. 952–985, May 2006.

Jiayang Wu received the B.S. degree in communication engineering in 2010 from Xidian University, Xian, China. He is currently working toward the Ph.D. degree at Shanghai Jiao Tong University, Shanghai, China. He has more than 30 publications in international journals and conferences, including *Journal of Lightwave Technology*, *Optics Express*, *Photonics Technology Letters*, and *Photonics Journal*. His current research interests include silicon photonics and nonlinear optics, especially with respect to on-chip all-optical computing and information processing.

Boyu Liu received the B.S. degree in 2013 from the Shanghai University of Science and Technology, Shanghai, China. He is currently working toward the M.S. degree at Shanghai Jiao Tong University, Shanghai. His current research interests include high-speed optical transmission systems and optical signal processing.

Jizong Peng received the B.S. degree in electronic engineering in 2014 from Shanghai Jiao Tong University, Shanghai, China. He is currently working toward the M.S. degree at Shanghai Jiao Tong University. His current research interests include high-speed optical transmission systems and optical signal processing.

Junming Mao received the B.S. degree in electronic science and technology in 2010 from East China Normal University, Shanghai, China. He is currently working toward the Ph.D. degree at Shanghai Jiao Tong University, Shanghai. His current research interests include silicon photonics and integrated optics.

Xinhong Jiang received the B.S. and M.S. degrees from Anhui University, Hefei, China, in 2009 and 2012, respectively. He is currently working toward the Ph.D. degree at Shanghai Jiao Tong University, Shanghai, China. His current research interests include optical signal processing and liquid-crystal photonic applications.

Ciyuan Qiu received the B.S. and M.S. degrees from Tsinghua University, Beijing, China, in 2005 and 2007, respectively, and the Ph.D. degree from Rice University, Houston, TX, USA, in 2013. He then worked as Postdoc at Rice University until June 2014. He is currently an Assistant Professor at Shanghai Jiao Tong University, Shanghai, China. He has been the author or coauthor of more than 20 journal articles and conference papers, such as *Nano Letters*, *Scientific Reports*, *Optics Letters*, and *Optics Express*.

His current research interests include silicon photonics devices and circuit, graphene optics, and plasmonics.

Christine Tremblay (M'02) received the B.S. degree in engineering physics from Université Laval, Québec, QC, Canada, in 1984, the M.Sc. degree from INRS-Énergie (Université du Québec), Varennes, QC, in 1985, and the Ph.D. degree from the École Polytechnique de Montréal, Montreal, QC, in 1992. From 1998 to 2004, she held senior R&D and technology management positions for four organizations. She was a Research Scientist with the National Optics Institute for eight years, Engineering Manager at EXFO (1998–2000), Product Manager for 40 G DWDM systems at Nortel (2000–2002), and Director of Engineering at Roctest (2002–2003). Since 2004, she is a Full Professor at the Department of Electrical Engineering, École de technologie supérieure (Université du Québec). She is the Founding Researcher and Head of the *Laboratoire de technologies de réseaux*. Her current research interests include coherent optical networks, performance monitoring, optical layer characterization, and silicon photonics. She is Coinstructor for OFC short courses SC314 (2009–) and SC210 (2011–) of the Optical Society of America (OSA). She is a Member of OSA, SYTACom and COPL. She served as a TPC Member of ACP 2013, and Scientific Committee Chair of SPIE Photonics North (2011, 2012) and ICT Workshop - Entretiens Jacques Cartier (2011, 2012).

Yikai Su (S'97–M'01–SM'07) received the B.S. degree from the Hefei University of Technology, Hefei, China, in 1991, the M.S. degree from the Beijing University of Aeronautics and Astronautics, Beijing, China, in 1994, and the Ph.D. degree in electronics engineering from Northwestern University, Evanston, IL, USA, in 2001. He worked at Crawford Hill Laboratory of Bell Laboratories before he joined the Shanghai Jiao Tong University, Shanghai, China, as a Full Professor in 2004. His current research interests include modulation formats, and silicon photonic devices for information transmission, switching, and processing. He has been the author or coauthor of more than 200 journal articles and conference papers. He is a Member of the Optical Society of America. He serves as an Associate Editor of *Photonic Research* (2013–), a Topical Editor of *Optics Letters* (2008–2014), a Guest Editor of IEEE JSTQE ON "NONLINEAR OPTICAL SIGNAL PROCESSING" in 2008/2011, and a Feature Editor of *Applied Optics* on the special issue of AOE 2008. He is the Chair of IEEE Photonics Society Shanghai chapter, a general cochair of ACP 2012, a TPC cochair of ACP 2011, and APCC 2009. He also served as a TPC member of a large number of international conferences including CLEO (2016–), ECOC (2013–2015), OFC (2011–2013), OECC 2008, CLEO-PR 2007, and LEOS (2005–2007).